Inorganic Chemistry

pubs.acs.org/IC

Article

Iridium(III)-Based Infrared Two-Photon Photosensitizers: Systematic Regulation of Their Photodynamic Therapy Efficacy

Xue-Lian Li, Li-Zhen Zeng, Rong Yang, Xu-Dan Bi, Yang Zhang, Ruo-Bing Cui, Xin-Xi Wu, and Feng Gao*

Cite This: *Inorg. Chem.* 2023, 62, 16122−16130

Read Online

ACCESS | Metrics & More | Article Recommendations | Supporting Information

ABSTRACT: Cyclometalated iridium(III) complexes are of significant importance in the field of antitumor photodynamic therapy (PDT), whether they exist as single molecules or are incorporated into nanomaterials. Nevertheless, a comprehensive examination of the relationship between their molecular structure and PDT effectiveness remains awaited. The influencing factors of two-photon excited PDT can be anticipated to be further multiplied, particularly in relation to intricate nonlinear optical properties. At present, a comprehensive body of research on this topic is lacking, and few discernible patterns have been identified. In this study, through systematic structure regulation, the nitro-substituted styryl group and 1-phenylisoquinoline ligand containing **YQ2** was found to be the most potent infrared two-photon excitable photosensitizer in a 4 × 3 combination library of cyclometalated Ir(III) complexes. **YQ2** could enter cells via an energy-dependent and caveolae-mediated pathway, bind specifically to mitochondria, produce $^1O_2$ in response to 808 nm LPL irradiation, activate caspases, and induce apoptosis. In vitro, **YQ2** displayed a remarkable phototherapy index for both malignant melanoma (>885) and non-small-cell lung cancer (>1234) based on these functions and was minimally deleterious to human normal liver and kidney cells. In in vivo antitumor phototherapy, **YQ2** inhibited tumor growth by an impressive 85% and could be eliminated from the bodies of mice with a half-life as short as 43 h. This study has the potential to contribute significantly to the development of phototherapeutic drugs that are extremely effective in treating large, profoundly located solid tumors as well as the understanding of the structure−activity relationship of Ir(III)-based PSs in PDT.

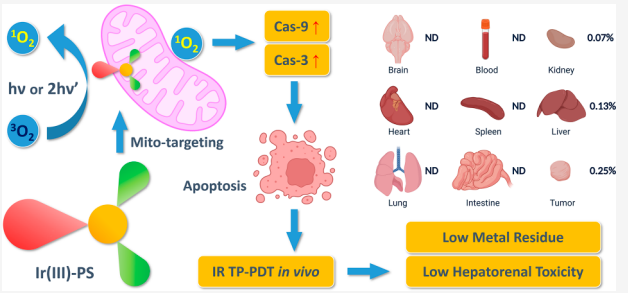

1. INTRODUCTION

Photodynamic therapy (PDT) is a promising approach for cancer treatment, wherein the activation of photosensitizers (PSs) by light irradiation leads to the generation of reactive oxygen species (ROS). This process ultimately induces the noninvasive eradication of tumor cells.[1,2] The functionality of PDT is, to a specific extent, dependent on the presence of oxygen.[3,4] The efficacy of PDT is significantly diminished in tumors, especially in large solid tumors, due to the presence of a hypoxic environment.[5,6] The integration of PDT with various other innovative therapeutic approaches, including photothermal therapy (PTT), photoacoustic therapy (PAT), photochemotherapy (PCT), and immunogenic cell death (ICD), has the potential to synergistically enhance treatment effectiveness and minimize the required dosage of therapeutic agents.[7−13] Taking a step back to assert, for PDT alone, the mechanisms underlying the construction of highly active molecules or materials through structural regulation are considered to be largely unidentified.[14,15]

Cyclometalated Ir(III) complexes, typically with one N^N main ligand for functions and two C^N ligands for ancillary modulation, are widely used as luminescent materials and antitumor PSs due to their extended triplet excited state (^{3}ES) lifetime and high quantum yield of both emission and ROS production, the vast majority of which is $^1O_2$.[16−18] As cationic complexes with optimized lipophilicity and cellular uptake, they are believed to be advantageous in PDT.[19−22] Despite recent advancements in the field, the development of new Ir(III)-PSs with customizable photophysical and photobiological characteristics has encountered certain challenges. These challenges include inadequate solubility in biological environments, resulting in low bioavailability, limited absorption, and quantum yield of $^1O_2$ generation within the PDT window of 700−1000 nm, and elevated toxicity toward normal cells.[23,24] A two-photon laser can overcome some of these limitations due to its better light penetration depth (allowing treatment of deeper tumors or lesions) and superior spatial

Received: July 12, 2023
Published: September 17, 2023

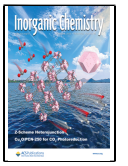

https://doi.org/10.1021/acs.inorgchem.3c02364
Inorg. Chem. 2023, 62, 16122−16130

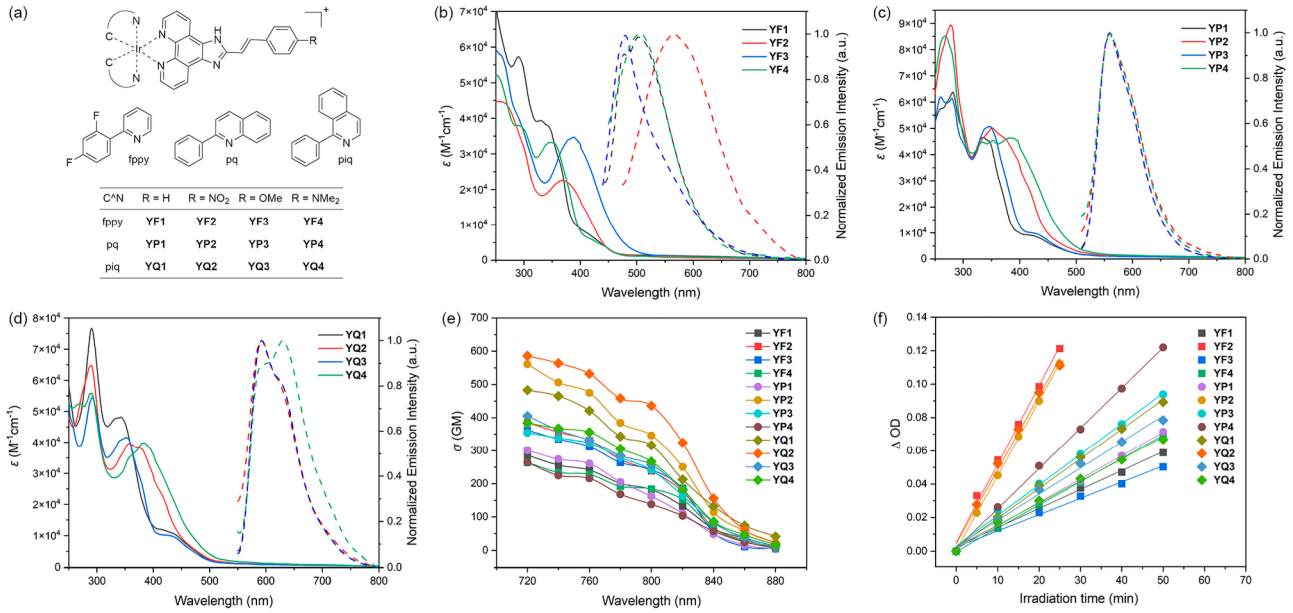

Figure 1. Structure and photophysical properties of infrared two-photon excitable Ir(III) photosensitizers (PSs) built in this study. (a) Structure of Ir(III)-PSs. (b) Absorption and emission spectra of **YF1−4** (10 μM) in aqueous solution. (c) Absorption and emission spectra of **YP1−4** (10 μM) in aqueous solution. (d) Absorption and emission spectra of **YQ1−4** (10 μM) in aqueous solution. (e) Two-photon absorption cross sections (TPACS, σ) of Ir(III)-PSs (50 μM in THF). (f) Singlet oxygen ($^1O_2$) generation upon 808 nm low-power laser (LPL, 100 mW cm^{-2}) irradiation in an aqueous solution.

selection (minimizing damage to surrounding healthy tissues). Nevertheless, it is worth noting that, in most documented cases involving TP-PDT, the excitation of the photosensitizer relies on the utilization of high-power laser irradiation. This approach results in local light intensities that significantly exceed the maximum permissible exposure (MPE) for skin under infrared (IR) light irradiation, as specified by the American national standard for safe use of lasers (ANSI Z136.1-2014) at a value of 0.33 W cm^{-2}. Consequently, this elevated light intensity has the potential to induce irreversible damage. Moreover, the complete coverage of solid tumors by the highly concentrated laser beam is severely limited, thereby significantly constraining its practicality. We have achieved successful dual TP-PDT and PTT through the utilization of a combination of a low-power laser (LPL, 808 nm, 100 mW cm^{-2}) with an adjustable spot-size (beam diameter >1.0 cm) as a light source and single-molecule Ru(II), Os(II), and Ir(III) complexes with extremely high TP absorption cross sections (TPACS) as both PSs and photothermal agents (PTAs).[25−28] The determination of photodynamic and photothermal properties is highly dependent on the allocation of excited state (ES) energy among various relaxation pathways, including radiative decay (luminescence), non-radiative (heat release), and energy transfer to oxygen (resulting in the production of $^1O_2$).

To better understand the correlation between the energy distribution tendency of ES and the structure of PS, especially under TP excitation by LPL, a systematic regulation of the structure of cyclometalated Ir(III) complexes has been carried out through a 4 × 3 combination library consisting of three C^N ligands and four N^N ligands (Figure 1a). Their photophysical properties, ES characteristics, photoexcited $^1O_2$ generation, cell uptake and mechanism, subcellular localization, and photoinduced apoptosis of the Ir(III)-PSs have been investigated. They exhibited a notable phototherapy index for malignant melanoma and non-small-cell lung cancer in both in vitro and in vivo environments. Regarding the safety of PSs, their potential residues within the body and hepatorenal toxicity were also tested. The representative PS **YQ2** could be eliminated from the bodies of mice quickly and demonstrated minimal toxicity toward normal liver and kidney cells. This study may contribute to the development of phototherapeutic drugs that are extremely effective in treating large, profoundly located solid tumors, as well as the understanding of the structure−activity relationship of Ir(III)-based PSs in PDT. In addition, it may offer new insights into the design strategies for TP-PSs concluded by various researchers to date.[29,30]

2. RESULTS AND DISCUSSION

2.1. Synthesis and Spectroscopy. The synthesis of Ir(III)-PSs **YF1−4**, **YP1−4**, and **YQ1−4** (at a yield of 62.6% to 91.7%) and their characterization (^{1}H NMR, ^{13}C NMR, ESI-MS, and microanalysis) are shown in the Supporting Information. As shown in Figure 1b−d, the absorption spectra of Ir(III)-PSs (10 μM in aqueous solution, solid lines) were quite adjustable by both the coordinated N^N ligands and the cyclometalated C^N ligands. From the simulated absorption spectra (Figures S1−S3), molecular orbital population (Figures S4−S6), and their comparisons with experimental data (Tables S1−S3), the absorption wavelengths and molar extinction coefficients (ε) were mainly affected by the intraligand (IL) transitions on the N^N ligands and metal-to-ligand charge transfer (MLCT) transitions between Ir(III) and N^N ligands.[31,32] The emission spectra of Ir(III)-PSs (10 μM in aqueous solution, Figure 1b−d, dashed lines) exhibited maximum emission wavelengths that increased from fppy to pq to piq for the effect of C^N ligands. Their emission properties were further studied by natural transition orbital (NTO) analysis (Figures S4−S6). For **YP1−4** and **YQ1−4**, the main emissive ESs were distributed on the C^N ligands and received less regulation from the N^N ligands. For **YF1−4**, however,

https://doi.org/10.1021/acs.inorgchem.3c02364
Inorg. Chem. 2023, 62, 16122−16130

Table 1. Photophysical and Photochemical Properties and in Vitro Photodynamic Therapeutic Activity of Ir(III)-PSs in This Study

PS	σ_{808} (GM)[a]	$\Phi_{\Delta 400}$[b]	$\Phi_{\Delta 808}$[b]	log $K_{O/W}$[c]	$IC_{50,TP}$ (μM)[d]	PI[d]	$IC_{50,TP\text{-}C}$ (μM)[d]	PI-C[d]
YF1	162	0.73	0.03	2.21	1.52 ± 0.13	>65.8	3.87 ± 0.24	>25.8
YF2	213	0.61	0.13	2.55	0.732 ± 0.051	>137	2.42 ± 0.16	>41.3
YF3	219	0.31	0.03	1.82	0.843 ± 0.062	>119	1.74 ± 0.14	>57.5
YF4	171	0.78	0.04	1.53	1.15 ± 0.09	>87.0	3.41 ± 0.26	>29.3
YP1	141	0.89	0.04	2.56	1.93 ± 0.14	>51.8	4.24 ± 0.32	>23.6
YP2	307	0.64	0.12	2.86	0.271 ± 0.030	>369	1.54 ± 0.12	>64.9
YP3	210	0.91	0.05	2.05	0.534 ± 0.041	>187	1.88 ± 0.16	>53.2
YP4	124	0.44	0.07	1.84	1.35 ± 0.11	>74.0	3.24 ± 0.22	>30.9
YQ1	275	0.82	0.05	2.83	1.07 ± 0.08	>93.5	2.82 ± 0.19	>35.5
YQ2	391	0.77	0.12	2.94	0.113 ± 0.012	>885	0.285 ± 0.023	>351
YQ3	242	0.83	0.04	2.36	0.265 ± 0.031	>377	1.53 ± 0.13	>65.4
YQ4	233	0.39	0.04	2.05	0.832 ± 0.064	>120	2.67 ± 0.24	>37.5
CP					1.32 ± 0.10	1.24	1.47 ± 0.11	1.12
5-ALA					68.7 ± 4.3	2.37	151 ± 12	1.08

[a]Two-photon absorption cross-section (TPASC) at 808 nm. [b]Singlet oxygen quantum yield in aqueous solution upon 400 nm LED (50 mW cm^{-2}, $\Phi_{\Delta 400}$) and 808 nm LPL (100 mW cm^{-2}, $\Phi_{\Delta 808}$) excitation. [c]*n*-Octanol and water distribution coefficient. [d]In vitro cytotoxicity upon 808 nm LPL (100 mW cm^{-2}, light dose = 30 J cm^{-2}) irradiation ($IC_{50,TP}$) and phototherapy index (PI, PI = $IC_{50,D}/IC_{50,TP}$) toward A375 human melanoma cell lines directly or covered by 1.0 mm thick chicken breast ($IC_{50,TP\text{-}C}$ and PI-C, PI-C = $IC_{50,D}/IC_{50,TP\text{-}C}$). Cytotoxicities of Ir(III)-PSs under dark conditions ($IC_{50,D}$) were tested to be >100 μM (solubility upper limit). The dark cytotoxicities of cisplatin (CP) and 5-ALA were tested to be 1.64 ± 0.11 and 163 ± 12, respectively.

most ESs with low energy level were contributed by the N^N ligands, resulting in a more obvious difference in emission wavelengths from each other.[33] All Ir(III)-PSs in this study exhibited a lifetime (τ) range from 814 to 970 ns in aqueous solution (Table S7), comparable to Ir(III)-PSs recently reported by different research groups.[7,27,34−38] Such a relatively long ES lifetime can facilitate photosensitization and photoinduced electron transfer processes on light activation.

2.2. Electrochemistry. The oxidative and reductive potentials (E_{ox} and E_{red}) of Ir(III)-PSs, as well as their differences (ΔE), were recorded in anhydrous MeCN by cyclic voltammetry and are summarized in Table S7. Typical irreversible Ir(IV)/Ir(III) oxidation couples were observed at 0.84−1.08 V, in accordance with cyclometalated Ir(III) complexes reported recently.[34,39] Introduction of the electron-withdrawing $-NO_2$ group on the N^N ligands did not lead to a perceptible enhancement in the electron-accepting ability and higher E_{ox} values of the PSs as expected,[26] whereas the E_{red} values shifted to the anode, rendering small ΔE values. From the population and energy level of the molecular orbitals (MOs, Figures S7 and S9), the lowest unoccupied MOs (LUMOs) of $-NO_2$ containing PSs were apparently lower than the others of the series. The DFT calculated energy gaps (E_{gap}, Table S7) between the highest occupied MO (HOMO) and LUMO also exhibited the same regularity. Such small E_{gap} and low excitation energy level ESs with IL characterizations may suggest a favorable efficacy of electron excitation and transfer for not only PSs in the PDT[1,40] but also Ir(III) photocatalysts in hydrogen evolution[41] and CO_2 reduction.[42]

2.3. Two-Photon Absorption. Beneficial from their excellent TPA properties, Ir(III)-PSs can nearly double their excitation wavelength from around 400 nm to near 800 nm, which greatly improved the light penetration into tissue and safety in phototherapeutic applications.[43,44] The TPASC (σ) is therefore an essential parameter for Ir(III)-PSs in TP-PDT. The Ir(III)-PSs in this study produce remarkable TP-induced fluorescence signals in the range of 720−880 nm with no apparent σ maxima (Figure 1e). The logarithm plots of the TP-induced fluorescence intensities (F) of Ir(III)-PSs exhibited a linear relationship to the excitation intensities at 800 nm (I) with slopes close to 2.0 (Figure S10), indicating the TPA characteristic.[45] Since many TPA-PSs with σ_{808} lower than 100 GM have been successfully applied in antitumor PDT, the Ru−Os complexes in this study can be expected to be more active in TP-excited antitumor PDT under 808 nm irradiation. The σ values at 808 nm (σ_{808}, Table 1) were 124−391 GM (1 GM = 10^{-50} cm^4 s $photon^{-1}$), which are not only higher than similar mononuclear Ir(III)[27,34,46] and Ru(II)[47−51] complexes at around 800 nm but quite comparable to certain dinuclear Ir(III),[52] Ru(II),[25,53] and Os(II)[54] complexes. Therefore, these Ir(III)-PSs can be expected to be potent TP-PSs that can be excited by an 808 nm LPL.

2.4. Photoexcited Singlet Oxygen Generation. The $^1O_2$ quantum yields (Φ_Δ) of a PS play an essential role in its photocytotoxicity. As depicted in Figures 1f and S11−S17, the absorbance of 9,10-anthracenediyl-bis(methylene)dimalonic acid (ABDA), a $^1O_2$ trapping probe, decreased rapidly under irradiation with a 400 nm LED (50 mW cm^{-2}) and 808 nm LPL (100 mW cm^{-2}) in the presence of Ir(III)-PSs, indicating the highly efficient generation of $^1O_2$. With the aid of a photon counting technique (detailed in the Supporting Information), the $^1O_2$ quantum yields under 400 nm (OP) and 808 nm (TP) excitation ($\Phi_{\Delta 400}$ and $\Phi_{\Delta 808}$, Table 1) could be calculated by taking into account the difference in photon numbers of excitation lights with various wavelengths. Ir(III)-PSs in this study showed remarkable $\Phi_{\Delta 400}$ values (0.31−0.91) in comparison to $\Phi_{\Delta 450}$ values (0.02−0.11) for styryl-containing Ru(II) complexes in aqueous solution under one-photon excitation,[49−51] indicating a high efficiency with which the energy of the excited state is transferred to $^1O_2$ through ^{3}IL during OP excitation. In the cases of TP excitation, $\Phi_{\Delta 808}$ values are apparently decreased. First, this is due to the TPA efficiency barrier, which means that not all 808 nm photons can be simultaneously absorbed in pairs and execute the excitation function. Second, the use of an IR LPL further reduces excitation efficiency, albeit increasing the feasibility

https://doi.org/10.1021/acs.inorgchem.3c02364
Inorg. Chem. 2023, 62, 16122−16130

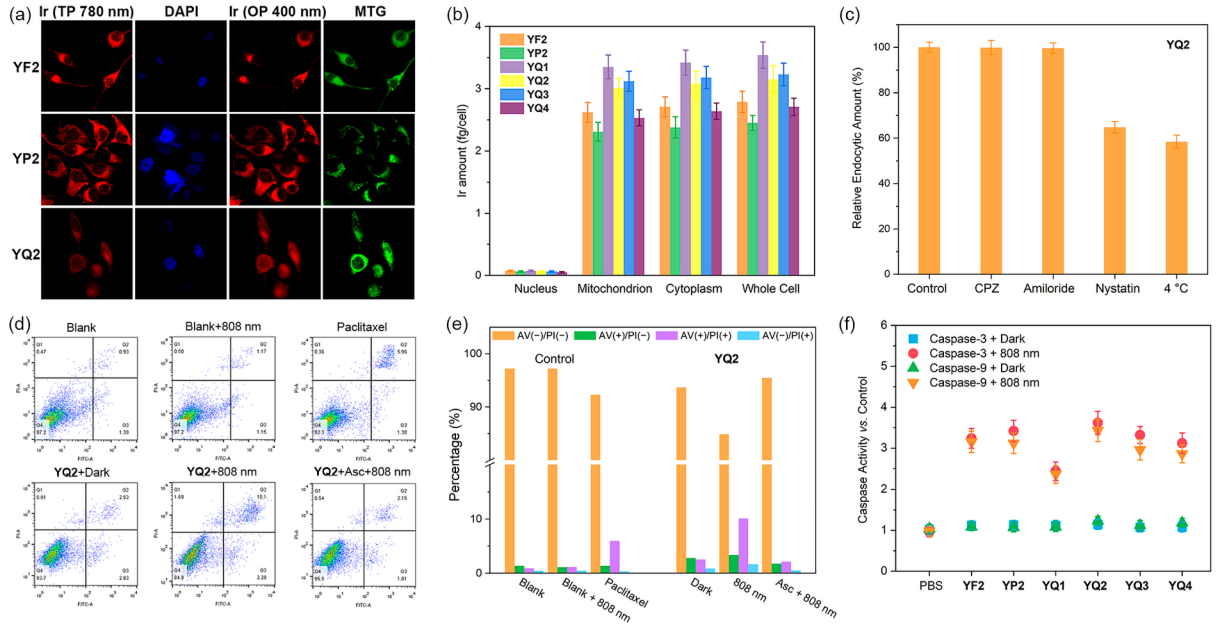

Figure 2. Subcellular distribution, cell uptake, and photoinduced apoptosis of selected Ir(III)-PSs toward the A375 human malignant melanoma cell line. (a) Mitochondria co-localization tested under one-photon (OP) and two-photon (TP) excitation by CLSM. (b) Cell uptake and distribution quantified by ICP-MS. (c) Relative endocytic amount of **YQ2** by A375 cells in the presence of chlorpromazine (CPZ, 10.0 μg mL^{-1}), amiloride (100.0 μg mL^{-1}), or nystatin (50.0 μg mL^{-1}) at 37 and 4 °C. (d and e) Flow cytometry detection of apoptosis in A375 cells (stained with Annexin V-FITC and PI) for the PDT treatments of **YQ2** (1 μM) in the dark or upon 808 nm LPL (100 mW cm^{-2}, light dose = 30 J cm^{-2}) irradiation. (f) Caspase activation of selected Ir(III)-PSs (1 μM) in A375 cells under the dark or upon 808 nm LPL (100 mW cm^{-2}, light dose = 30 J cm^{-2}) irradiation.

and safety of TP phototherapy. Finally, the upper limit of $\Phi_{\Delta 808}$ should be 0.5, according to the definition of quantum yield, since TP excitation requires the absorption of two photons by the PS to produce one $^1O_2$.

The $\Phi_{\Delta 808}$ values of Ir(III)-PSs are quite remarkable (0.03−0.13), in comparison to $[Ru(bpy)_3]^{2+}$ (0.006), a series of dinuclear[25] and mononuclear homoligand[26] Ru(II)-PSs (0.020−0.156), heterocyclic containing Ir(III)-PSs (0.026−0.110),[27] and Ru(II)−Os(II) heteronuclear PSs (0.06−0.32)[28] under identical experimental conditions. Interestingly, the $\Phi_{\Delta 808}$ values of Ir(III)-PSs exhibited an ignorable correlation with $\Phi_{\Delta 400}$ but more consistent with the regularity of σ_{808}. The $-NO_2$ group containing **YF2**, **YP2**, and **YQ2** showed much higher $\Phi_{\Delta 808}$ than the other PSs, which was speculated to be due to their higher σ_{808}. It indicates that the $^1O_2$ yield of a TPA-PS under TP excitation may be more determined by its TPA capacity than by its ES property and transition nature under OP excitation.

2.5. Photothermal Conversion. Some Ir(III) complexes can exert excellent photothermal conversion efficiency (PCE) under 808 nm LPL irradiation when encapsulated as nanomaterials or aggregates[55−58] and more recently in a single-molecule state[27] via the ES vibration relaxation.[59] The Ir(III)-PSs in this study did not exhibit notable photothermal conversion (PTC) ability even when exposed to an 808 nm LPL at a relative high power (1.0 W cm^{-2}). The temperature increases of the aqueous solutions (PBS) of Ir(III)-PSs were identical to those of the PBS control (Figure S17). Classic metal complex prototypes, such as $[Ru(bpy)_3]^{2+}$ (bpy = 2,2′-bipyridine), $[Ru(bpy)_2(dppz)]^{2+}$ (dppz = dipyrido[3,2-*a*:2′,3′-*c*]phenazine), $[Ru(bpy)_2(pip)]^{2+}$ (pip = 2-phenyl-imidazo[4,5-*f*][1,10]phenanthroline), $[Ir(ppy)_2(bpy)]^{2+}$ (ppy = 2-phenylpyridine), $[Ir(ppy)_2(pip)]^{2+}$, etc., also exhibited ignorable PCEs. This highlights the necessity of the structurally movable (vibration or rotatory) groups in PSs for non-radiative decay (heat release).[60] Therefore, the Ir(III)-PSs in this study can produce remarkable $^1O_2$ upon 808 nm LPL (100 mW cm^{-2}) irradiation with no PTC effect, supporting their application as highly efficient and safe PDT reagents.

2.6. In Vitro Cytotoxicity. Since irradiation around 400 nm (one-photon excitation wavelengths for Ir(III)-PSs) can directly induce cell damage, only 808 nm LPL (100 mW cm^{-2}) irradiation was used to assess photocytotoxicity upon two-photon excitation. In both human melanoma cells A375 (Table 1) and human lung cancer cells A549 (Table S8), all Ir(III)-PSs displayed ignorable cytotoxicity at their respective limits of solubility (100 μM) under dark conditions while exhibiting notable photocytotoxicities as determined by the CCK-8 assay. The $-NO_2$ group and piq ligand-containing PSs (**YF2**, **YP2**, and **YQ1**−**4**) showed much higher phototoxicities than the other PSs, which was speculated to be due to their higher $\Phi_{\Delta 808}$ and σ_{808}. **YQ2** achieved quite remarkable phototherapy indexes (PIs) of 885 for A375 cells and 1234 for A549 cells, making it one of the most efficient phototherapeutic metal complexes and materials ever discovered. Under the same conditions, the FDA-approved PDT drug 5-ALA exhibited reduced phototoxicity and PI. As a chemotherapeutic agent, cisplatin (CP) did not show an apparent change in cytotoxicity (PI = 1.15−1.62) under either irradiated or non-irradiated conditions. The photostability of Ir(III)-PSs has been examined in cell medium (RMPI-1640) under 808 nm laser irradiation for 5 min (identical light dose used in in vitro and in vivo PDT study). From Figure S19, the Ir(III)-PSs have good stability and photostability under these physiological conditions.

https://doi.org/10.1021/acs.inorgchem.3c02364
Inorg. Chem. 2023, 62, 16122−16130

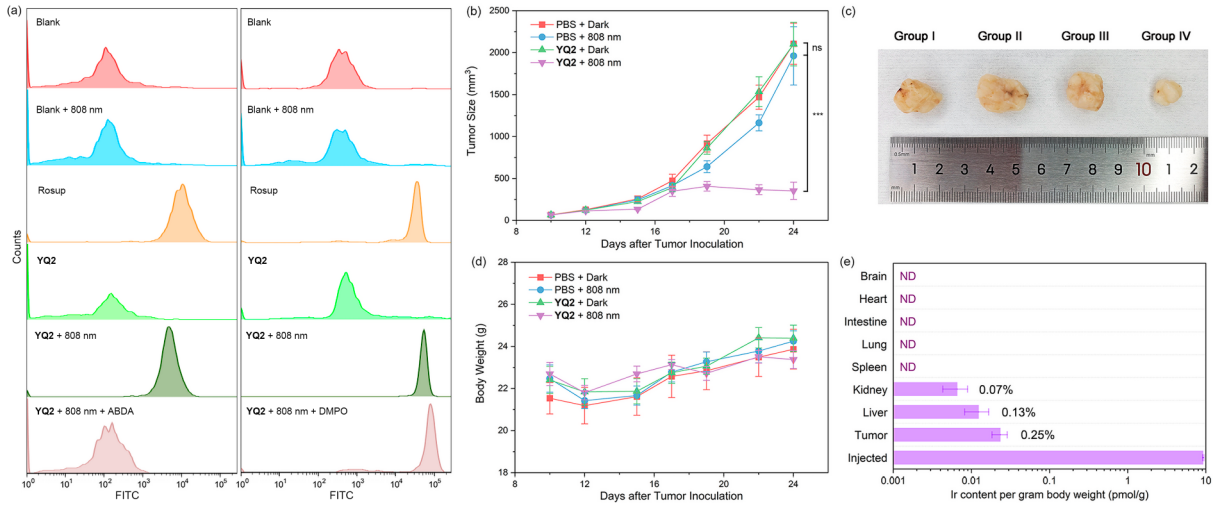

Figure 3. Intracellular $^1O_2$ generation and in vivo TP-PDT of **YQ2** toward BALB/c nude mice (subcutaneous A375 human melanoma xenograft model). (a) Intracellular ROS detection by flow cytometry. Blank represents A375 cells alone. Rosup is the positive control of ROS. ABDA and DMPO are $^1O_2$ and $O_2^{\bullet-}$ scavengers, respectively. (b) Histogram of the mean tumor volume for the four groups. $p < 0.05$ was the accepted level of significance. ns: not significant. *** $p < 0.001$. (c) Photograph of representative post-treatment A375 tumors for each group. (d) Histogram of mean body weight for the four groups. (e) Iridium residues in the collected organs in **YQ2**-injected groups (Group III and IV, 14 days after injection). ND: not detected.

By covering the cell plates with a 1.0 mm thick chicken breast during photoirradiation, it was possible to evaluate the viability of the tissue penetration for deep-seated tumor phototherapy by the Ir(III)-PSs. Under these conditions, the photocytotoxicity of PSs experienced a reduction of approximately two-thirds, primarily attributed to the impact of tissue on the processes of light absorption, reflection, and scattering. Relying on their own extremely high σ_{808} values, their photocytotoxicity remained at a higher level compared to similar photosensitizers. The ability of **YQ2** to exert a high PDT activity (PI-CC = 351 for A375 and 541 for A549 cell lines) under 808 nm LPL irradiation even when covered by 1.0 mm of physiological tissue is crucial for realistic drug applications in vivo.

2.7. Subcellular Localization and Cell Uptake. The effectiveness of PDT is significantly influenced by the cell uptake and intracellular distribution of PSs.[61−65] Therefore, the subcellular localization of the Ir(III)-PSs was further studied. As shown in Figures 2a and S20, all Ir(III)-PSs showed bright luminescence within cells. The signals exhibited a significant degree of overlap well with the mitochondrial dye MTG, suggesting a propensity for targeting mitochondria in cells. When excited by a TP (780 nm) laser, the Ir(III)-PSs showed identical localization to those under OP excitation (400 nm), suggesting an effective excitation of PSs within living cells. A possible reason for the near absence of Ir(III)-PSs in the nuclei may be attributed to their ignorable DNA affinity, as suggested by the absorption spectroscopic titration (Figure S21) and DNA thermal denaturation (Figure S22).

The cell uptake and endocytic pathway were further investigated in PSs with higher PIs (**YF2**, **YP2**, and **YQ1**−**4**). ICP-MS results suggest that all PSs were taken up by cells efficiently (Figure 2b). This may be due to their felicitous lipophilicity (oil−water partition coefficient, log $K_{O/W}$ = 1.0−3.0, Table 1 and Figure S23), which is proven to be beneficial to both a balanced volume of distribution and the potential for good absorption and bioavailability.[66] Their distribution in mitochondria accounted for up to 94% of the total cellular uptake. **YQ2** showed decreased uptake at 4 °C or in the presence of the caveolae formation inhibitor nystatin (Figure 2c), while it was not affected by the clathrin vesicle formation inhibitor chlorpromazine (CPZ) or the macropinocytic pathway inhibitor amiloride, indicating that **YQ2** entered the cell via caveolae-mediated and energy-dependent pathways. The efficient transmembrane transport undoubtedly ensured the PSs' ability to function effectively within cells.

2.8. Apoptosis and Caspase Activation. Melanoma cells may go through the mitochondrial mechanism of apoptosis when exposed to photogenerated $^1O_2$.[67] Annexin V-FITC/propidium iodide (PI) staining was utilized to examine **YQ2**-induced apoptosis in A375 cell lines during TP-PDT (Figure 2d). Figure 2e illustrates the data for each quadrant. Under dark settings, **YQ2**-treated melanoma cells displayed patterns that were quite similar to those of untreated cells (blank). The late apoptotic percentages of **YQ2**-treated cells increased after irradiation, indicating that they may activate apoptosis in melanoma cells. Caspase-9 (Cas-9) initiates a cascade of subsequent caspase processing events throughout the apoptotic process by directly cleaving and activating Cas-3 and Cas-7 to trigger cell death.[68,69] Cas-3 and Cas-9 activation was determined in PS-treated melanoma cells (Figure 2f). Under dark conditions, neither caspase was activated in all PS-treated cells. With 808 nm irradiation, the activities of both Cas-3 and Cas-9 significantly increased. These findings point to a photodependent apoptosis mechanism, most likely via intracellular photogenerated $^1O_2$, in the PS-containing melanoma cells. This photoinduced apoptosis mechanism may contribute substantially to the highly efficient PDT activity of Ir(III)-PSs.

Recently, it has been discovered that certain Ir(III)-PSs can induce cell ferroptosis by increasing oxidative stress by ROS generation in tumor cells, lowering glutathione (GSH) levels, and subsequently promoting membrane lipid peroxidation.[70,71] The GSH and lipid peroxide (LPO) levels in PBS- or **YQ2**-treated A375 cells exposed to 808 nm LPL irradiation or kept in the dark were tested by commercial kits. As depicted in Figure S24, neither a significant amount of LPO nor an evident

https://doi.org/10.1021/acs.inorgchem.3c02364
Inorg. Chem. 2023, 62, 16122−16130

suppression of GSH was detected in **YQ2**-treated A375 cells under irradiation or in the dark, indicating that **YQ2** is not a ferroptosis photoinducing reagent. Moreover, autophagy (3-methyladenine, 3-MA), necrosis (necrostatin-1, Nec-1), and paraptosis (cycloheximide, CHX) inhibitors had no discernible effect on the viability of **YQ2**-treated A375 cells (Figure S25), suggesting that **YQ2** may not induce cell death via these mechanisms.[50]

2.9. Intracellular $^1O_2$ Generation. Given that the Ir(III)-PSs can generate $^1O_2$ efficiently in the aqueous solution upon 808 nm LPL irradiation and be taken up by A375 cells efficiently, $^1O_2$ generation of **YQ2** in A375 cells was studied using DCFH-DA (2′,7′-dichlorodihydrofluorescein diacetate) as a ROS detector and Rosup as a positive control. As evidenced by the flow cytometry histograms (Figure 3a), ROS was observed exclusively when both **YQ2** and 808 nm LPL irradiation were present. The absence of light under the experimental conditions of **YQ2** prevented the generation of ROS, possibly contributing to the diminutive dark toxicity observed in the in vitro cell viability assay. In the presence of $^1O_2$ trapping probe ABDA, all ROS-induced signals were completely suppressed, whereas the signal intensity was hardly affected in the presence of an $O_2^{\bullet-}$ scavenger, 5,5-dimethyl-1-pyrroline-1-oxide (DMPO), in 100-fold excess. It suggests that, in comparison to electron transfer processes (Type I) which are initiated by $O_2 + e \rightarrow O_2^{\bullet-}$, and subsequently generate ROS and RNS like H_2O_2, $OH^{\bullet}$, and $ONOO^-$, etc., the energy transfer process (Type II) dominates **YQ2**'s intracellular ROS production and PDT activity.

2.10. In Vivo PDT. Mice bearing A375 tumors (BALB/c mouse model with tumor xenografts) were divided into different groups based on the drug administered. Mice were intratumorally injected with PBS (Groups I and II) or **YQ2** (Groups III and IV), irradiated with 808 nm LPL (Groups II and IV, 100 mW cm^{-2}, light dose = 30.0 J cm^{-2}) or kept unirradiated (Groups I and III). There were no instances of skin injury observed during the phototherapy sessions in this study. This can be attributed to the fact that the irradiation of 808 nm LPL used in this study was kept below 30% of the MPE standard for 808 nm laser exposure to skin. Following a 14-day period, the average volume (V) of tumors in Groups I–III reached 2000 mm^3, as depicted in Figure 3b and c. Additionally, there was no observed decline in the body weight of the mice, as illustrated in Figure 3d. These findings suggest that the systemic toxicity of **YQ2** in mice in the absence of irradiation is remarkably minimal. The **YQ2**-treated group subjected to irradiation (Group IV) exhibited a significant antitumor effect, as evidenced by a tumor volume measurement of 300 mm^3 and an inhibition rate of 85% (Figure 3b and c). The observed variations in hematoxylin and eosin (H&E) staining patterns between Group IV tumor sections and the remaining samples indicate that **YQ2**-mediated TP-PDT has the potential to induce destruction of tumor tissues. Conversely, the H&E staining of sections obtained from the principal organs (Figure S26) did not reveal any significant lesions, thus confirming the absence of toxicity associated with **YQ2** in vivo.

2.11. Biodistribution and Hepato-/Nephrotoxicity Evaluation. A significant safety concern associated with pharmaceuticals containing metals is the potential risk that heavy metals pose to the human body, specifically the liver and kidneys. The existing research has predominantly concentrated on evaluating the efficacy of drug delivery to tumors within a few hours following administration in animal models. Nevertheless, there has been a notable lack of attention given to the examination of residual substances and the potential presence of toxic elements following the treatment process. The present study utilized ICP-MS to quantitatively determine the remaining amount of iridium in the organs and tumors obtained from mice that were injected with **YQ2**, 14 d after administration (Figure 3e). Notably, trace quantities of iridium were identified in tumors, kidneys, and livers, whereas no detectable levels were observed in any other organs. The clearance of **YQ2** from the body is more efficient compared to cisplatin, Photofrin II, and porfimer sodium from the respective half-lives $t_{1/2}$ of 58–73, >100, and 250 h. This is demonstrated by the mean total residue of 0.45% observed in ten mice injected with **YQ2** ($t_{1/2}$ = 43 h). The short half-life of **YQ2** following PDT offers clear benefits in terms of rapid elimination, thereby reducing the occurrence of adverse effects, such as photodermatosis.

To ascertain the potential hepatotoxic and nephrotoxic effects of the residue, an investigation was conducted to evaluate the toxicities of **YQ2** and cisplatin on human normal liver (HL-7702) and kidney (HK-2) cells. Based on the results of in vitro cytotoxicity tests, **YQ2** has negligible cytotoxic effects on A375, HL-7702, and HK-2 cells when not exposed to irradiation (Figure S27a). At concentrations ranging from 1 to 10 μM, which is approximately 5–6 orders of magnitude higher than the overall residue of **YQ2** found in mice, the viability of normal cells remained above 99 to 94% (Figure S27b and c). In contrast, cisplatin demonstrates a substantial ability to suppress the proliferation of A375 cells and a certain degree of toxicity in HL-7702 and HK-2 cells (Figure S27b and c). This allows **YQ2** to achieve a state of relative safety prior to its complete eradication from the organism.

3. CONCLUSIONS

In conclusion, by systematic regulation of the structure, the nitro-substituted styryl group and piq ligand containing **YQ2** have been found to be the most potent infrared two-photon excitable PS among a series of Ir(III) complexes. **YQ2** could enter cells by an energy-dependent and caveolae-mediated pathway, specifically bind to mitochondria, generate $^1O_2$ upon 808 nm LPL irradiation, activate caspases, and induce apoptosis. Based on these functions, **YQ2** exhibited quite a remarkable phototherapy index for both malignant melanoma (>885) and non-small-cell lung cancer (>1234) and minimal toxicity to human normal liver and kidney cells in vitro. In in vivo antitumor phototherapy, **YQ2** exhibited a high inhibition rate of 85% in tumor size and could be eliminated from the bodies of mice quite efficiently with a half-life of 43 h. The results of this study have the potential to make a significant contribution toward the advancement of phototherapeutic drugs that are highly effective in treating large, deeply located solid tumors, as well as the structure–activity relationship of cyclometalated Ir(III) complexes in PDT.

4. EXPERIMENTAL SECTION

The experimental details including materials, instruments, synthesis, characterization, DFT calculations, singlet oxygen quantum yield, lipophilicity ($\log K_{o/w}$), photothermal conversion efficiency, subcellular co-localization, cell uptake, in vitro cytotoxicity, flow cytometry analysis, caspase activation, and in vivo PDT are given in the Supporting Information.

https://doi.org/10.1021/acs.inorgchem.3c02364
Inorg. Chem. 2023, 62, 16122–16130

■ ASSOCIATED CONTENT

Supporting Information

The Supporting Information is available free of charge at https://pubs.acs.org/doi/10.1021/acs.inorgchem.3c02364.

Synthesis and characterizations, simulated and experimental absorption spectra, photostability, plots of excited state transitions, DNA-binding experiments, quantum yield determination for the $^1O_2$ generation, DNA photocleavage, oil/water partition, and experimental and computational absorption spectral data of Ir(III) complexes (PDF)

■ AUTHOR INFORMATION

Corresponding Author

Feng Gao − *Key Laboratory of Medicinal Chemistry for Natural Resource, Ministry of Education; Yunnan Provincial Center for Research & Development of Natural Products; School of Pharmacy, Yunnan University, Kunming 650500, P. R. China*; orcid.org/0000-0001-7490-4887; Email: gaofeng@ynu.edu.cn

Authors

Xue-Lian Li − *Key Laboratory of Medicinal Chemistry for Natural Resource, Ministry of Education; Yunnan Provincial Center for Research & Development of Natural Products; School of Pharmacy, Yunnan University, Kunming 650500, P. R. China*

Li-Zhen Zeng − *Key Laboratory of Medicinal Chemistry for Natural Resource, Ministry of Education; Yunnan Provincial Center for Research & Development of Natural Products; School of Pharmacy, Yunnan University, Kunming 650500, P. R. China*

Rong Yang − *Key Laboratory of Medicinal Chemistry for Natural Resource, Ministry of Education; Yunnan Provincial Center for Research & Development of Natural Products; School of Pharmacy, Yunnan University, Kunming 650500, P. R. China*

Xu-Dan Bi − *Key Laboratory of Medicinal Chemistry for Natural Resource, Ministry of Education; Yunnan Provincial Center for Research & Development of Natural Products; School of Pharmacy, Yunnan University, Kunming 650500, P. R. China*

Yang Zhang − *Key Laboratory of Medicinal Chemistry for Natural Resource, Ministry of Education; Yunnan Provincial Center for Research & Development of Natural Products; School of Pharmacy, Yunnan University, Kunming 650500, P. R. China*

Ruo-Bing Cui − *Key Laboratory of Medicinal Chemistry for Natural Resource, Ministry of Education; Yunnan Provincial Center for Research & Development of Natural Products; School of Pharmacy, Yunnan University, Kunming 650500, P. R. China*

Xin-Xi Wu − *Key Laboratory of Medicinal Chemistry for Natural Resource, Ministry of Education; Yunnan Provincial Center for Research & Development of Natural Products; School of Pharmacy, Yunnan University, Kunming 650500, P. R. China*

Complete contact information is available at: https://pubs.acs.org/10.1021/acs.inorgchem.3c02364

Notes

The authors declare no competing financial interest.

■ ACKNOWLEDGMENTS

This work was supported by National Natural Science Foundation of China (22167022), Yunnan Provincial Science and Technology Department (2018FB022), and Youth Talents Project of Yunnan Province (YNWR-QNBJ-2018-057). The authors thank the Advanced Analysis and Measurement Center of Yunnan University for their help in characterization. The Table of Contents graphic was created with BioRender.com.

■ REFERENCES

(1) Monro, S.; Colon, K. L.; Yin, H. M.; Roque, J.; Konda, P.; Gujar, S.; Thummel, R. P.; Lilge, L.; Cameron, C. G.; McFarland, S. A. Transition Metal Complexes and Photodynamic Therapy from a Tumor-Centered Approach: Challenges, Opportunities, and Highlights from the Development of TLD1433. *Chem. Rev.* **2019**, *119* (2), 797−828.

(2) Feng, J.; Ren, W.-X.; Kong, F.; Dong, Y.-B. Recent insight into functional crystalline porous frameworks for cancer photodynamic therapy. *Inorg. Chem. Front.* **2021**, *8* (4), 848−879.

(3) Wu, H.; Wang, L.; Wang, Y.; Shao, Y.; Li, G.; Shao, K.; Akkaya, E. U. Targeted Singlet Oxygen Delivery: A Bioorthogonal Metabolic Shunt Linking Hypoxia to Fast Singlet Oxygen Release. *Angew. Chem., Int. Ed.* **2022**, *61* (47), No. e202210249.

(4) Chen, W.; Wang, Z.; Tian, M.; Hong, G.; Wu, Y.; Sui, M.; Chen, M.; An, J.; Song, F.; Peng, X. Integration of TADF Photosensitizer as "Electron Pump" and BSA as "Electron Reservoir" for Boosting Type I Photodynamic Therapy. *J. Am. Chem. Soc.* **2023**, *145* (14), 8130−8140.

(5) Woods, J. J.; Wilson, J. J. A Dinuclear Persulfide-Bridged Ruthenium Compound is a Hypoxia-Selective Hydrogen Sulfide (H2S) Donor. *Angew. Chem., Int. Ed.* **2021**, *60* (3), 1588−1592.

(6) Wang, H.; Xue, K. F.; Yang, Y. C.; Hu, H.; Xu, J. F.; Zhang, X. In Situ Hypoxia-Induced Supramolecular Perylene Diimide Radical Anions in Tumors for Photothermal Therapy with Improved Specificity. *J. Am. Chem. Soc.* **2022**, *144* (5), 2360−2367.

(7) Karges, J. Clinical Development of Metal Complexes as Photosensitizers for Photodynamic Therapy of Cancer. *Angew. Chem., Int. Ed.* **2022**, *61* (5), No. e202112236.

(8) Lee, L. C.-C.; Lo, K. K.-W. Luminescent and Photofunctional Transition Metal Complexes: From Molecular Design to Diagnostic and Therapeutic Applications. *J. Am. Chem. Soc.* **2022**, *144* (32), 14420−14440.

(9) Manzano, C. M.; Nakahata, D. H.; de Paiva, R. E. F. Revisiting metallodrugs for the treatment of skin cancers. *Coord. Chem. Rev.* **2022**, *462*, No. 214506.

(10) Huang, L.; Leung, P. K.-K.; Lee, L. C.-C.; Xu, G.-X.; Lam, Y.-W.; Lo, K. K.-W. Photofunctional cyclometallated iridium(iii) polypyridine methylsulfone complexes as sulfhydryl-specific reagents for bioconjugation, bioimaging and photocytotoxic applications. *Chem. Commun.* **2022**, *58* (73), 10162−10165.

(11) Ling, Y.-Y.; Kong, Y.-J.; Hao, L.; Pan, Z.-Y.; Mao, Z.-W.; Tan, C.-P. Photodegradation of carbonic anhydrase by iridium complexes for induction of immunogenic cell death under hypoxia. *Inorg. Chem. Front.* **2023**, *10* (11), 3284−3292.

(12) Vigueras, G.; Markova, L.; Novohradsky, V.; Marco, A.; Cutillas, N.; Kostrhunova, H.; Kasparkova, J.; Ruiz, J.; Brabec, V. A photoactivated Ir(iii) complex targets cancer stem cells and induces secretion of damage-associated molecular patterns in melanoma cells characteristic of immunogenic cell death. *Inorg. Chem. Front.* **2021**, *8* (21), 4696−4711.

(13) Ke, L.; Wei, F.; Xie, L.; Karges, J.; Chen, Y.; Ji, L.; Chao, H. A Biodegradable Iridium(III) Coordination Polymer for Enhanced Two-Photon Photodynamic Therapy Using an Apoptosis-Ferroptosis Hybrid Pathway. *Angew. Chem., Int. Ed.* **2022**, *61* (28), No. e202205429.

(14) Roque, J. A., III; Cole, H. D.; Barrett, P. C.; Lifshits, L. M.; Hodges, R. O.; Kim, S.; Deep, G.; Frances-Monerris, A.; Alberto, M. E.; Cameron, C. G.; McFarland, S. A. Intraligand Excited States Turn

a Ruthenium Oligothiophene Complex into a Light-Triggered Ubertoxin with Anticancer Effects in Extreme Hypoxia. *J. Am. Chem. Soc.* **2022**, *144* (18), 8317−8336.
(15) Cole, H. D.; Roque, J. A., III; Shi, G.; Lifshits, L. M.; Ramasamy, E.; Barrett, P. C.; Hodges, R. O.; Cameron, C. G.; McFarland, S. A. Anticancer Agent with Inexplicable Potency in Extreme Hypoxia: Characterizing a Light-Triggered Ruthenium Ubertoxin. *J. Am. Chem. Soc.* **2022**, *144* (22), 9543−9547.
(16) Liu, S.; Han, J.; Chang, Y.; Wang, W.; Wang, R.; Wang, Z.; Li, G.; Zhu, D.; Bryce, M. R. AIE-active iridium(iii) complex integrated with upconversion nanoparticles for NIR-irradiated photodynamic therapy. *Chem. Commun.* **2022**, *58* (72), 10056−10059.
(17) Fan, Z.; Rong, Y.; Sadhukhan, T.; Liang, S.; Li, W.; Yuan, Z.; Zhu, Z.; Guo, S.; Ji, S.; Wang, J.; Kushwaha, R.; Banerjee, S.; Raghavachari, K.; Huang, H. Single-Cell Quantification of a Highly Biocompatible Dinuclear Iridium(III) Complex for Photocatalytic Cancer Therapy. *Angew. Chem., Int. Ed.* **2022**, *61* (23), No. e202202098.
(18) Pei, Y.; Sun, Y.; Huang, M.; Zhang, Z.; Yan, D.; Cui, J.; Zhu, D.; Zeng, Z.; Wang, D.; Tang, B. Ir(III) Complexes with AIE Characteristics for Biological Applications. *Biosensors* **2022**, *12* (12), 1104.
(19) Wang, Z.; Li, L.; Wang, W.; Wang, R.; Li, G.; Bian, H.; Zhu, D.; Bryce, M. R. Self-assembled nanoparticles based on cationic mono-/AIE tetra-nuclear Ir(iii) complexes: long wavelength absorption/near-infrared emission photosensitizers for photodynamic therapy. *Dalton Trans.* **2023**, *52* (6), 1595−1601.
(20) Liu, S.; Han, J.; Wang, W.; Chang, Y.; Wang, R.; Wang, Z.; Li, G.; Zhu, D.; Bryce, M. R. AIE-active Ir(iii) complexes functionalised with a cationic Schiff base ligand: synthesis, photophysical properties and applications in photodynamic therapy. *Dalton Trans.* **2022**, *51* (42), 16119−16125.
(21) Hou, B.; Zhang, W.; Li, C.; Sun, X.; Feng, X.; Liu, J. Synthesis and in vitro biological evaluation of novel water-soluble porphyrin complexes for cancer photodynamic therapy. *Appl. Organomet. Chem.* **2022**, *36* (4), No. e6598.
(22) Daniels, R. E.; McKenzie, L. K.; Shewring, J. R.; Weinstein, J. A.; Kozhevnikov; Valery, N.; Bryant, H. E. Pyridazine-bridged cationic diiridium complexes as potential dual-mode bioimaging probes. *RSC Adv.* **2018**, *8* (18), 9670−9676.
(23) Li, B. H.; Liu, H. K.; He, Y. L.; Zhao, M. Y.; Ge, C.; Younis, M. R.; Huang, P.; Chen, X. Y.; Lin, J. A ″Self-Checking″ pH/Viscosity-Activatable NIR-II Molecule for Real-Time Evaluation of Photothermal Therapy Efficacy. *Angew. Chem., Int. Ed.* **2022**, *61* (16), No. e202200025.
(24) Ge, H.; Du, J.; Long, S.; Xia, X.; Zheng, J.; Xu, N.; Yao, Q.; Fan, J.; Peng, X. Near-Infrared Light Triggered H2 Generation for Enhanced Photothermal/Photodynamic Therapy against Hypoxic Tumor. *Adv. Healthc. Mater.* **2022**, *11* (3), No. 2101449.
(25) Wang, M.-F.; Yang, R.; Tang, S.-J.; Deng, Y.-A.; Li, G.-K.; Zhang, D.; Chen, D.; Ren, X.; Gao, F. In vivo Realization of Dual Photodynamic and Photothermal Therapy for Melanoma by Mitochondria Targeting Dinuclear Ruthenium Complexes under Civil Infrared Low-power Laser. *Angew. Chem., Int. Ed.* **2022**, *61* (38), No. e202208721.
(26) Tang, S.-J.; Wang, M.-F.; Yang, R.; Liu, M.; Li, Q.-F.; Gao, F. More-Is-Better Strategy for Constructing Homoligand Polypyridyl Ruthenium Complexes as Photosensitizers for Infrared Two-Photon Photodynamic Therapy. *Inorg. Chem.* **2023**, *62* (21), 8210−8218.
(27) Tang, S.-J.; Li, Q.-F.; Wang, M.-F.; Yang, R.; Zeng, L.-Z.; Li, X.-L.; Wang, R.-D.; Zhang, H.; Ren, X.; Zhang, D.; Gao, F. Bleeding the Excited State Energy to the Utmost: Single-Molecule Iridium Complexes for In Vivo Dual Photodynamic and Photothermal Therapy by an Infrared Low-Power Laser. *Adv. Healthc. Mater.* **2023**, No. 2301227.
(28) Deng, Y.-A.; Tang, S.-J.; Wang, M.-F.; Ren, X.; Li, X.-L.; Zeng, L.-Z.; Ren, D.-N.; Wang, M.-R.; Xiao, W.-L.; Cai, Z.-Y.; Zhang, D.; Zhang, H.; Gao, F. Heterometallic ruthenium-osmium complexes: dual photodynamic and photothermal therapy for melanoma and drug-resistant lung tumor in vivo. *Inorg. Chem. Front.* **2023**, *10* (15), 4552−4561.
(29) Karges, J.; Chao, H.; Gasser, G. Critical discussion of the applications of metal complexes for 2-photon photodynamic therapy. *JBIC Journal of Biological Inorganic Chemistry* **2020**, *25* (8), 1035−1050.
(30) Pawlicki, M.; Collins, H. A.; Denning, R. G.; Anderson, H. L. Two-Photon Absorption and the Design of Two-Photon Dyes. *Angew. Chem., Int. Ed.* **2009**, *48* (18), 3244−3266.
(31) Chen, X.; Gao, F.; Yang, W.-Y.; Zhou, Z.-X.; Lin, J.-Q.; Ji, L.-N. Structure□Activity Relationship of Polypyridyl Ruthenium(II) Complexes as DNA Intercalators, DNA Photocleavage Reagents, and DNA Topoisomerase and RNA Polymerase Inhibitors. *Chem. Biodiver.* **2013**, *10* (3), 367−384.
(32) Sun, J.; Wu, S.; Chen, H.-Y.; Gao, F.; Liu, J.; Ji, L.-N.; Mao, Z.-W. Synthesis, characterization and DNA-binding and DNA-photocleavage studies of two Ru(II) complexes containing two main ligands and one ancillary ligand. *Polyhedron* **2011**, *30* (12), 1953−1959.
(33) Tao, P.; Lv, Z.; Zheng, X.-K.; Jiang, H.; Liu, S.; Wang, H.; Wong, W.-Y.; Zhao, Q. Isomer Engineering of Lepidine-Based Iridophosphors for Far-Red Hypoxia Imaging and Photodynamic Therapy. *Inorg. Chem.* **2022**, *61* (44), 17703−17712.
(34) Bi, X.-D.; Yang, R.; Zhou, Y.-C.; Chen, D.; Li, G.-K.; Guo, Y.-X.; Wang, M.-F.; Liu, D.; Gao, F. Cyclometalated Iridium(III) Complexes as High-Sensitivity Two-Photon Excited Mitochondria Dyes and Near-Infrared Photodynamic Therapy Agents. *Inorg. Chem.* **2020**, *59* (20), 14920−14931.
(35) Gourdon, L.; Cariou, K.; Gasser, G. Phototherapeutic anticancer strategies with first-row transition metal complexes: a critical review. *Chem. Soc. Rev.* **2022**, *51* (3), 1167−1195.
(36) Liu, Y.-Y.; Yu, H.-J.; Wang, Y.-P.; Li, C.-J.; Wang, X.-F.; Ye, C.-G.; Yao, H.-L.; Pan, M.; Su, C.-Y. A photoactive Ir−Pd bimetallic cage with high singlet oxygen yield for efficient one/two-photon activated photodynamic therapy. *Materials Chemistry Frontiers* **2022**, *6* (7), 948−955.
(37) Lu, X.; Xiong, C.; Li, B.; Du, W.; Li, D.; Ma, W.; Tian, X.; Tian, Y.; Zhang, Q. Three-photon absorption iridium(iii) photosensitizers featuring aggregation induced emission. *Inorg. Chem. Front.* **2022**, *9* (9), 1890−1896.
(38) Mizukami, K.; Muraoka, T.; Shiozaki, S.; Tobita, S.; Yoshihara, T. Near-Infrared Emitting Ir(III) Complexes Bearing a Dipyrromethene Ligand for Oxygen Imaging of Deeper Tissues In Vivo. *Anal. Chem.* **2022**, *94* (6), 2794−2802.
(39) Yoon, S.; Gray, T. G.; Teets, T. S. Enhanced Deep-Red Phosphorescence in Cyclometalated Iridium Complexes with Quinoline-Based Ancillary Ligands. *Inorg. Chem.* **2023**, *62* (20), 7898−7905.
(40) Yin, H.; Stephenson, M.; Gibson, J.; Sampson, E.; Shi, G.; Sainuddin, T.; Monro, S.; McFarland, S. A. In vitro multiwavelength PDT with 3IL states: teaching old molecules new tricks. *Inorg. Chem.* **2014**, *53* (9), 4548−4559.
(41) Wang, Y.; Huang, Y.; Chen, S.; Gao, J.; Zhang, Y.; Duan, Y.-c.; Deng, P. Construction of Robust Iridium(III) Complex-Based Photosensitizer for Boosting Hydrogen Evolution. *Inorg. Chem.* **2023**, *62* (19), 7212−7219.
(42) Lee, D.; Choe, M. S.; Lee, H. J.; Shin, J. Y.; Kim, C. H.; Son, H.-J.; Kang, S. O. Accumulative Charge Separation in a Modular Quaterpyridine Bridging Ligand Platform and Multielectron Transfer Photocatalysis of π-Linked Dinuclear Ir(III)−Re(I) Complex for CO2 Reduction. *Inorg. Chem.* **2023**, *62* (22), 8445−8461.
(43) Vickerman, B. M.; Zywot, E. M.; Tarrant, T. K.; Lawrence, D. S. Taking phototherapeutics from concept to clinical launch. *Nat. Rev. Chem.* **2021**, *5* (11), 816−834.
(44) Dąbrowski, J. M.; Pucelik, B.; Regiel-Futyra, A.; Brindell, M.; Mazuryk, O.; Kyzioł, A.; Stochel, G.; Macyk, W.; Arnaut, L. G. Engineering of relevant photodynamic processes through structural modifications of metallotetrapyrrolic photosensitizers. *Coord. Chem. Rev.* **2016**, *325*, 67−101.
(45) Bin, F.-C.; Guo, M.; Li, T.; Zheng, Y.-C.; Dong, X.-Z.; Liu, J.; Jin, F.; Zheng, M.-L. Carbazole-based Anion Ionic Water-Soluble

https://doi.org/10.1021/acs.inorgchem.3c02364
Inorg. Chem. 2023, 62, 16122−16130

Two-Photon Initiator for Achieving 3D Hydrogel Structures. *Adv. Funct. Mater.* **2023**, No. 2300293.
(46) Colombo, A.; Dragonetti, C.; Roberto, D.; Valore, A.; Ferrante, C.; Fortunati, I.; Picone, A. L.; Todescato, F.; Williams, J. A. G. Two-photon absorption properties and 1O2 generation ability of Ir complexes: an unexpected large cross section of [Ir(CO)2Cl(4-(para-di-n-butylaminostyryl)pyridine)]. *Dalton Trans.* **2015**, *44* (35), 15712−15720.
(47) Wang, H.; Tian, X.; Guan, L.; Zhang, Q.; Zhang, S.; Zhou, H.; Wu, J.; Tian, Y. Targeting mitochondrial DNA with a two-photon active Ru(ii) phenanthroline derivative. *J. Mater. Chem. B* **2016**, *4* (17), 2895−2902.
(48) Zhang, Q.; Tian, X.; Zhou, H.; Wu, J.; Tian, Y. Lighting the Way to See Inside Two-Photon Absorption Materials: Structure−Property Relationship and Biological Imaging. *Materials* **2017**, *10* (3), 223.
(49) Vinck, R.; Karges, J.; Tharaud, M.; Cariou, K.; Gasser, G. Physical, spectroscopic, and biological properties of ruthenium and osmium photosensitizers bearing diversely substituted 4,4′-di(styryl)-2,2′-bipyridine ligands. *Dalton Trans.* **2021**, *50* (41), 14629−14639.
(50) Karges, J.; Kuang, S.; Ong, Y. C.; Chao, H.; Gasser, G. One- and Two-Photon Phototherapeutic Effects of RuII Polypyridine Complexes in the Hypoxic Centre of Large Multicellular Tumor Spheroids and Tumor-Bearing Mice**. *Chem. Eur. J.* **2021**, *27* (1), 362−370.
(51) Karges, J.; Kuang, S.; Maschietto, F.; Blacque, O.; Ciofini, I.; Chao, H.; Gasser, G. Rationally designed ruthenium complexes for 1- and 2-photon photodynamic therapy. *Nat. Commun.* **2020**, *11* (1), 3262.
(52) Xu, W. J.; Liu, S. J.; Zhao, X.; Zhao, N.; Liu, Z. Q.; Xu, H.; Liang, H.; Zhao, Q.; Yu, X. Q.; Huang, W. Synthesis, One- and Two-Photon Photophysical and Excited-State Properties, and Sensing Application of a New Phosphorescent Dinuclear Cationic Iridium(III) Complex. *Chem. Eur. J.* **2013**, *19* (2), 621−629.
(53) Hanczyc, P.; Norden, B.; Samoc, M. Two-photon absorption of metal-organic DNA-probes. *Dalton Trans.* **2012**, *41* (11), 3123−3125.
(54) Wang, M.-F.; Deng, Y.-A.; Li, Q.-F.; Tang, S.-J.; Yang, R.; Zhao, R.-Y.; Liu, F.-D.; Ren, X.; Zhang, D.; Gao, F. Dinuclear osmium complexes as mitochondrion-targeting antitumor photothermal agents in vivo. *Chem. Commun.* **2022**, *58* (91), 12676−12679.
(55) Zhang, L. P.; Geng, Y.; Li, L. J.; Tong, X. F.; Liu, S.; Liu, X. M.; Su, Z. M.; Xie, Z. G.; Zhu, D. X.; Bryce, M. R. Rational design of iridium-porphyrin conjugates for novel synergistic photodynamic and photothermal therapy anticancer agents. *Chem. Sci.* **2021**, *12* (16), 5918−5925.
(56) Liu, B.; Jiao, J.; Xu, W.; Zhang, M.; Cui, P.; Guo, Z.; Deng, Y.; Chen, H.; Sun, W. Highly Efficient Far-Red/NIR-Absorbing Neutral Ir(III) Complex Micelles for Potent Photodynamic/Photothermal Therapy. *Adv. Mater.* **2021**, *33* (32), No. e2100795.
(57) Zhao, J.; Yan, K.; Xu, G.; Liu, X.; Zhao, Q.; Xu, C.; Gou, S. An Iridium (III) Complex Bearing a Donor−Acceptor−Donor Type Ligand for NIR-Triggered Dual Phototherapy. *Adv. Funct. Mater.* **2021**, *31* (11), No. 2008325.
(58) Shen, J.; Karges, J.; Xiong, K.; Chen, Y.; Ji, L.; Chao, H. Cancer cell membrane camouflaged iridium complexes functionalized black-titanium nanoparticles for hierarchical-targeted synergistic NIR-II photothermal and sonodynamic therapy. *Biomaterials* **2021**, *275*, No. 120979.
(59) Li, X.; Lovell, J. F.; Yoon, J.; Chen, X. Clinical development and potential of photothermal and photodynamic therapies for cancer. *Nat. Rev. Clin. Oncol.* **2020**, *17* (11), 657−674.
(60) Xi, D.; Xiao, M.; Cao, J.; Zhao, L.; Xu, N.; Long, S.; Fan, J.; Shao, K.; Sun, W.; Yan, X.; Peng, X. NIR Light-Driving Barrier-Free Group Rotation in Nanoparticles with an 88.3% Photothermal Conversion Efficiency for Photothermal Therapy. *Adv. Mater.* **2020**, *32* (11), No. 1907855.
(61) Zhu, J.-H.; Xu, G.-X.; Shum, J.; Lee, L. C.-C.; Lo, K. K.-W. Tuning the organelle specificity and cytotoxicity of iridium(iii) photosensitisers for enhanced phototheranostic applications. *Chem. Commun.* **2021**, *57* (90), 12008−12011.
(62) Wang, K.-N.; Liu, L.-Y.; Mao, D.; Hou, M.-X.; Tan, C.-P.; Mao, Z.-W.; Liu, B. A Nuclear-Targeted AIE Photosensitizer for Enzyme Inhibition and Photosensitization in Cancer Cell Ablation. *Angew. Chem., Int. Ed.* **2022**, *61* (15), No. e202114600.
(63) Liu, C. X.; Wang, B.; Zhu, W. P.; Xu, Y. F.; Yang, Y. Y.; Qian, X. H. An Endoplasmic Reticulum (ER)-Targeting DNA Nanodevice for Autophagy-Dependent Degradation of Proteins in Membrane-Bound Organelles. *Angew. Chem., Int. Ed.* **2022**, *61* (38), No. e202205509.
(64) Heng, H.; Song, G.; Cai, X.; Sun, J.; Du, K.; Zhang, X.; Wang, X.; Feng, F.; Wang, S. Intrinsic Mitochondrial Reactive Oxygen Species (ROS) Activate the In Situ Synthesis of Trimethine Cyanines in Cancer Cells. *Angew. Chem., Int. Ed.* **2022**, *61* (38), No. e202203444.
(65) Ma, Z.; Han, H.; Zhao, Y. Mitochondrial dysfunction-targeted nanosystems for precise tumor therapeutics. *Biomaterials* **2023**, *293*, No. 121947.
(66) Stocks, M. Chapter 3 - The small molecule drug discovery process − from target selection to candidate selection. In *Introduction to Biological and Small Molecule Drug Research and Development*; Ganellin, R., Roberts, S., Jefferis, R., Eds.; Elsevier: 2013; pp 81−126.
(67) Novikova, I. N.; Potapova, E. V.; Dremin, V. V.; Dunaev, A. V.; Abramov, A. Y. Laser-induced singlet oxygen selectively triggers oscillatory mitochondrial permeability transition and apoptosis in melanoma cell lines. *Life Sci.* **2022**, *304*, No. 120720.
(68) Cullen, S. P.; Martin, S. J. Caspase activation pathways: some recent progress. *Cell Death Differ.* **2009**, *16* (7), 935−938.
(69) Pérez-Hernández, M.; del Pino, P.; Mitchell, S. G.; Moros, M.; Stepien, G.; Pelaz, B.; Parak, W. J.; Gálvez, E. M.; Pardo, J.; de la Fuente, J. M. Dissecting the Molecular Mechanism of Apoptosis during Photothermal Therapy Using Gold Nanoprisms. *ACS Nano* **2015**, *9* (1), 52−61.
(70) Wang, W.-J.; Ling, Y.-Y.; Zhong, Y.-M.; Li, Z.-Y.; Tan, C.-P.; Mao, Z.-W. Ferroptosis-Enhanced Cancer Immunity by a Ferrocene-Appended Iridium(III) Diphosphine Complex. *Angew. Chem., Int. Ed.* **2022**, *61* (16), No. e202115247.
(71) Ke, L.; Wei, F.; Xie, L.; Karges, J.; Chen, Y.; Ji, L.; Chao, H. A Biodegradable Iridium(III) Coordination Polymer for Enhanced Two-Photon Photodynamic Therapy Using an Apoptosis−Ferroptosis Hybrid Pathway. *Angew. Chem., Int. Ed.* **2022**, *61* (28), No. e202205429.

https://doi.org/10.1021/acs.inorgchem.3c02364
Inorg. Chem. 2023, 62, 16122−16130